

SANDIA REPORT

SAND2000-1337

Unlimited Release

Printed June 2000

Integration of Optoelectronics and MEMS by Free-Space Micro-optics

M. E. Warren, O. Spahn, W. C. Sweatt, R. J. Shul, J. R. Wendt, G. A. Vawter,
T. W. Krygoski, D. Reyes, S. M. Rodgers and J. J. Sniegowski

Prepared by
Sandia National Laboratories
Albuquerque, New Mexico 87185 and Livermore, California 94550

Sandia is a multiprogram laboratory operated by Sandia Corporation,
a Lockheed Martin Company, for the United States Department of
Energy under Contract DE-AC04-94AL85000.

A disclosure of invention relating to the subject of this publication has
been filed with the U.S. Department of Energy.

Approved for public release; further dissemination unlimited.



Sandia National Laboratories

Issued by Sandia National Laboratories, operated for the United States Department of Energy by Sandia Corporation.

NOTICE: This report was prepared as an account of work sponsored by an agency of the United States Government. Neither the United States Government, nor any agency thereof, nor any of their employees, nor any of their contractors, subcontractors, or their employees, make any warranty, express or implied, or assume any legal liability or responsibility for the accuracy, completeness, or usefulness of any information, apparatus, product, or process disclosed, or represent that its use would not infringe privately owned rights. Reference herein to any specific commercial product, process, or service by trade name, trademark, manufacturer, or otherwise, does not necessarily constitute or imply its endorsement, recommendation, or favoring by the United States Government, any agency thereof, or any of their contractors or subcontractors. The views and opinions expressed herein do not necessarily state or reflect those of the United States Government, any agency thereof, or any of their contractors.

Printed in the United States of America. This report has been reproduced directly from the best available copy.

Available to DOE and DOE contractors from
U.S. Department of Energy
Office of Scientific and Technical Information
P.O. Box 62
Oak Ridge, TN 37831

Telephone: (865)576-8401
Facsimile: (865)576-5728
E-Mail: reports@adonis.osti.gov
Online ordering: <http://www.doe.gov/bridge>

Available to the public from
U.S. Department of Commerce
National Technical Information Service
5285 Port Royal Rd
Springfield, VA 22161

Telephone: (800)553-6847
Facsimile: (703)605-6900
E-Mail: orders@ntis.fedworld.gov
Online order: <http://www.ntis.gov/ordering.htm>



SAND2000-1337
Unlimited Release
Printed June 2000

Integration of Optoelectronics and MEMS by Free-Space Micro-optics

M. E. Warren, O. Spahn and W. C. Sweatt
Photonics Research Department

R. J. Shul, J. R. Wendt and G. A. Vawter
Compound Semiconductor Materials and Processes Department

T. W. Krygowski, D. Reyes, S. M. Rodgers and J. J. Sniegowski
Intelligent Micromachines Department

Sandia National Laboratories
P.O. Box 5800
Albuquerque, NM 87185-0603

Abstract

This report represents the completion of a three-year Laboratory-Directed Research and Development (LDRD) program to investigate combining microelectromechanical systems (MEMS) with optoelectronic components as a means of realizing compact optomechanical subsystems. Some examples of possible applications are laser beam scanning, switching and routing and active focusing, spectral filtering or shuttering of optical sources. The two technologies use dissimilar materials with significant compatibility problems for a common process line. This project emphasized a hybrid approach to integrating optoelectronics and MEMS. Significant progress was made in developing processing capabilities for adding optical function to MEMS components, such as metal mirror coatings and through-vias in the substrate. These processes were used to demonstrate two integration examples, a MEMS discriminator driven by laser illuminated photovoltaic cells and a MEMS shutter or chopper. Another major difficulty with direct integration is providing the optical path for the MEMS components to interact with the light. We explored using folded optical paths in a transparent substrate to provide the interconnection route between the components of the system. The components can be surface-mounted by flip-chip bonding to the substrate. Micro-optics can be fabricated into the substrate to reflect and refocus the light so that it can propagate from one device to another and then be directed out of the substrate into free space. The MEMS components do not require the development of transparent optics and can be completely compatible with the current 5-level polysilicon process. We report progress on a MEMS-based laser scanner using these concepts.

Keywords: microelectromechanical systems, MEMS, micro-optoelectromechanical systems, MOEMS, optoelectronics, optical integration, microsystem, deep reactive ion etching, VCSEL, hybrid package, diffractive optical element.

Acknowledgements

The authors would like to thank J.J. Smith, now with Allied Signal, for helpful discussions, H.Q. Hou, now with Emcore, and K.D. Choquette for use of 1.06 micron VCSELs. The authors would also like to thank T.R. Carter and G.Grossetete for their expert assistance in characterizing the performance of the devices and S. Samora, J. Banas and C.G. Willison, for expert support in the fabrication and process development. We would like to thank D.J. Rieger and J.S. Wheeler for their development of the solder processes and R.E. Asbill for flip-chip bonding support. Sandia is a multiprogram laboratory operated by Sandia Corporation, a Lockheed Martin Company, for the United States Department of Energy under Contract DE-AC04-94AL85000...

Introduction

Sandia is currently a world leader in two rapidly-developing technologies, vertical-cavity surface-emitting lasers (VCSELs) and microelectromechanical systems (MEMS). This project started as a means of coupling those two efforts together to enable development of combined systems and subsystems that allow the direct mechanical manipulation of light beams for a wide range of applications. Since the manipulation of light does not require large forces or torques and small motions can be amplified by longer beam paths, optical applications are ideal for demonstrating the capabilities of the current MEMS technology. Combining MEMS with optoelectronic components is a means of realizing miniature electrooptical and optomechanical subsystems that have great potential in weapon system and environmental sensor applications. Some subsystem examples are laser beam scanning, switching and routing and active focusing, spectral filtering or shuttering of a laser or other sources. A major obstacle to realizing these types of systems in a single structure is the difficulty of integrating the processing of the two classes of devices. The incompatibilities include dissimilar materials systems, with different processing temperature ranges and with significant cross-contamination problems for a common process line. Another major difficulty with direct integration of the two types of devices is providing the optical path for the MEMS components to interact with the light source. It is currently difficult to fabricate transparent optical components in conventional MEMS technology for use in the visible and near infrared where many applications are of interest. This limits the usefulness of simply stacking one device on top of another without a means of getting light through the MEMS substrate.

One hybrid approach to the integration of optoelectronics and MEMS that has been popularized is the “silicon optical bench” approach in which simple analogs of common optical bench components, such as tilting mirror mounts, are fabricated by MEMS technology on the surface of a wafer with the optical path limited to a horizontal plane a hundred microns or so above the wafer surface. This approach is a good demonstration of the capabilities of MEMS, but has

severe limitations for practical optical systems. The devices are usually hand “assembled” on probe stations because of the complex and space-consuming actuator technology needed to erect the components into working position. More limiting are the constraints on the optical system, since the beam cannot be allowed to expand to a radius larger than the center height of the erected MEMS optical components without unacceptable losses and coherent noise. This is a fundamental problem, given the diffractive properties of light, especially for highly divergent sources like the edge-emitting diode lasers that are currently used. These systems will also be very difficult to package and very susceptible to surface contamination and dust.

The system design approach in this project uses folded optical paths in a transparent substrate to provide the interconnection route between the components of the system. The active components can be surface-mounted by flip-chip bonding to the substrate. Micro-optics can be fabricated into the substrate to reflect and refocus the light at precise angles and, with transparent potting materials, the light paths can be completely confined inside solid materials until final output from the system. The 3-dimensional nature of the optical interconnection of the components gives the technique great flexibility for sophisticated systems. The MEMS components do not require the development of transparent optical elements and can be completely compatible with the current 5-level polysilicon process in the MDL. The optoelectronic devices can be VCSEL or detector arrays that are ideally suited for surface-mounting. The required micro-optical elements were developed at Sandia for other applications . A complete tool set of design and fabrication capabilities exists for transparent and reflecting elements that can direct the light through the system efficiently. Fused silica is the most appealing substrate material because of its compatibility with visible wavelength. For long wavelength applications, semiconductor substrates are perfectly suitable.

Realization of these types of micro-optical systems requires some additional capabilities in the processing of the MEMS devices. Much of this project has concentrated on developing

additional processing steps that can be performed on the silicon MEMS components after the major fabrication activities in the Microelectronics Development Laboratory (MDL) have been completed. These additional processing steps allow for metallic mirror coatings and special etching of the substrate of the MEMS wafer to improve the optical functionality of the devices. Because of incompatibilities with the processing line used for MEMS, these processes were developed at the Compound Semiconductor Research Laboratory (CSRL). This type of processing has been dubbed “postprocessing” or “back-end-of-line” processing to indicate its relationship to the rest of the MEMS process flow.

Postprocessing of Silicon MEMS

An important requirement for implementing optical functions in MEMS is the ability to make good mirrors on the polysilicon surfaces. A shadow mask technique that is applicable to released MEMS parts has been demonstrated. Some of the challenges included designing a process which would allow evaporation of Au on a previously released MEMS structure, without affecting its ability to move. Furthermore, since the release processing included coating with self-assembled monolayers, there was a possibility that the evaporated metal might not stick to the MEMS surfaces. This was found not to be a problem, since good adhesion was achieved upon evaporation of 80 Å of Ti and 500 Å of Au. Another potential issue was the possibility of warp induced in the thin polysilicon structures upon evaporation due to stress caused by the metal film, which would prevent them from moving. Due to the low stress recipe used for evaporation, this problem was avoided.

Flip-chip bonding is a key technology in this project for assembling the dissimilar parts together, or onto common substrates, for building subsystems. Early in the project, we flip-chip bonded visible wavelength VCSELs to fused silica substrates (which had etched microlenses) with an older flip-chip system. This was a successful demonstration of our ability to accomplish such

assemblies, but also indicated the need for a more precise system to achieve the alignment tolerances of a few microns that is often needed. A new flip-chip aligner was purchased for this and other programs. Initial results with bonding GaAs chips to GaAs chips and GaAs chips to fused silica substrates are very encouraging. Ultimately, solder bump bonding, in which solder bumps are fabricated for flip-chip bonding and solder reflow helps pull the parts into alignment, may be the preferred technique for assembling these structures.

Another key processing goal is fabrication of high efficiency diffractive optical elements in the polysilicon MEMS structures. The granular nature of polysilicon was cause for some concern as to whether our dry etch processes could provide surfaces smooth enough, after etching, to make high efficiency diffractive optics. The atomic force microscopy capability in the CSRL was used to make a study of surface roughness of polysilicon etched with chlorine-based reactive ion beam etching, (RIBE). The most promising approach is to use polysilicon surfaces smoothed by chemical-mechanical polishing in the MDL. Etching a diffractive optical pattern into the polished surface with RIBE resulted in very little surface roughness. The CMP polysilicon samples had initial RMS roughness values of 4-5 nm. After RIBE etching, the etched surfaces showed comparable to slightly less surface roughness of 3-4 nm. Later in this report we describe how we have realized high efficiency diffractive elements in polysilicon with this process.

After postprocessing steps have been performed, cross contamination concerns usually prohibit further processing of the devices in the MDL. Process development has involved development of release and drying processes in the CSRL in order to complete metallization and via formation prior to the release of the MEMS sample. A crucial step following the release process involves drying. Two methods were implemented: sublimation drying and self-assembled monolayer (SAM) coatings. The goal of both of these methods is the removal of the final rinse H₂O without collapsing the MEMS parts due to capillary action. Sublimation drying was found to work in a satisfactory fashion on 4-level MEMS, however it did not work on 5-level MEMS. These latter

MEMS structure needed SAM coatings in order to sufficiently dry as well as provide additional lubrication. In addition, a pre-release metallization process was implemented. This process involves deposition of several hundred Å of Au on a clean polysilicon surface. One of the difficulties overcome was selective removal of oxide over the polysilicon areas that were to be covered by Au. A bi-layer metal mask had to be used in order to protect the SiO₂ from an HF etch in the areas without Au. However once the desired Au thickness was evaporated on polysilicon, it did not have to be protected against the release etch, greatly simplifying the process. Figure 1 shows one of the released and dried dual pop-up mirrors with Au on it in a popped-up position.

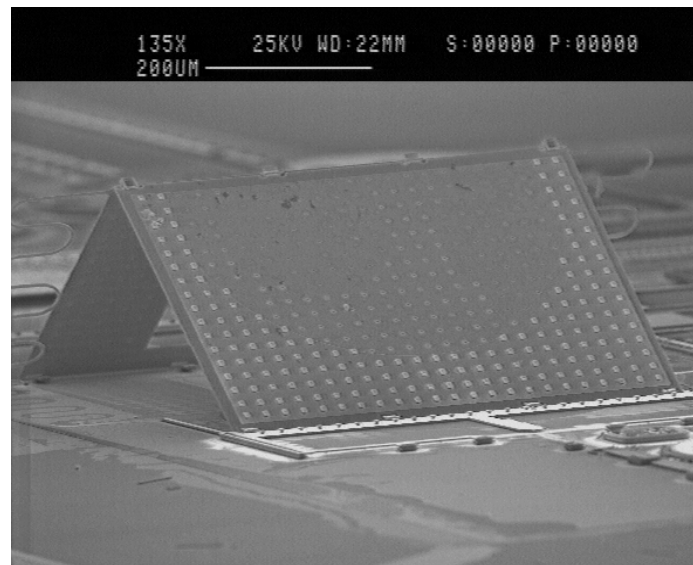


Figure 1. Scanning electron microscope view of the metallized pop-up MEMS mirror.

We have implemented vias in the substrate of the MEMS structures for optical access. This was accomplished by first depositing temporary metal alignment marks on the front of the wafer in order to use the backside mask aligner to align the via pattern on the back of the wafer into a proper position under the mirror. Then a thick photoresist was deposited on the back to protect the wafer where there were to be no vias and the remaining areas were etched using the deep Si etch process in the CSRL¹. One of the resulting vias is shown in Figure 2. These optical

photomicrographs show the backside of the wafer with a via. Through the hole, the backside of the mirror, and in particular the hinges, are visible. This wafer was not yet released and the via etch stopped on the SiO₂/SiN layer underneath the polysilicon layers comprising the MEMS structure.

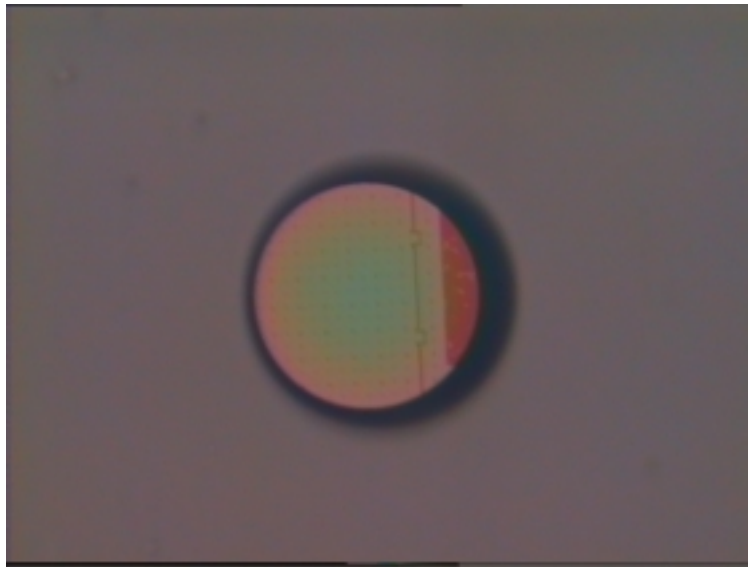
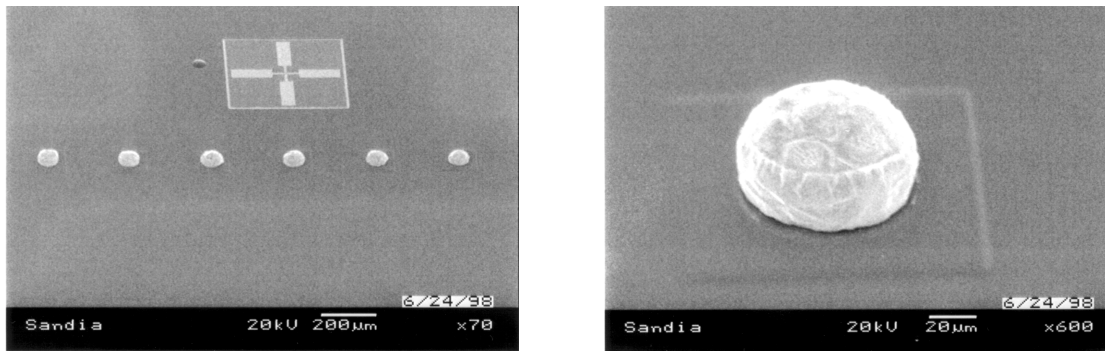


Figure 2. An optical microscope view of an etched via from the back side of a MEMS chip. The unreleased polysilicon MEMS structure is visible in the bottom of the via.

Another major activity was in development of flip-chip bonding processes using the flip-chip aligner. The work was primarily on gold thermo-compression bonding for bonding VCSELs to substrates. This method is reasonably reliable and is a quick method of flip-chip bonding parts. Destructive shear testing has shown that this method yields a low strength bond when there are a small number of bonds on the parts. Studies in underfilling with a clear adhesive for VCSELs were performed. The advantages of underfill are improved bond strength and better optical coupling between the VCSEL and the substrates. Destructive testing on these parts has shown shear strengths of 20 to 45 lbs. Unfortunately, we have not yet found a transparent underfill that does not show high shrinkage, stressing the die and the bonds.

A solder bump process was partly developed as well. The tin/lead solder electroplating process deposits 60-40 tin/lead solder to form a plug-like structure, which is defined by photoresist. After removal of the photoresist and seed layer, the structure is reflowed to form a solder ball. We used a previously developed reflow process that uses formic acid as a flux. The formic acid is transported to the substrate in a vapor phase with N₂ as the carrier gas. Reflow temperatures as low as 220C have been demonstrated. The concentration of the formic acid is 2% and appears to have no residue that would be detrimental to an optical interface. Figure 3a shows a row of solder balls after reflow. The balls are on gold pads on fused silica substrates. Figure 3b shows a closeup of a single solder ball. A polyimide solder dam layer covers the substrate except for the regions contacted by the solder balls.



Figures 3a and 3b. 3a (left) shows a row of solder bumps formed by electroplating and fluxless reflow. 3b (right) is a closeup of a single solder ball.

Combined Photonics and MEMS Function Demonstrations

In this section we describe efforts in integrating MEMs and photonic functions and discusses the fabrication constraints on both system components. We describe two demonstrations where photonic and MEMS technologies have been integrated to show proof-of-principle functionality for possible weapon-related mechanical functions².

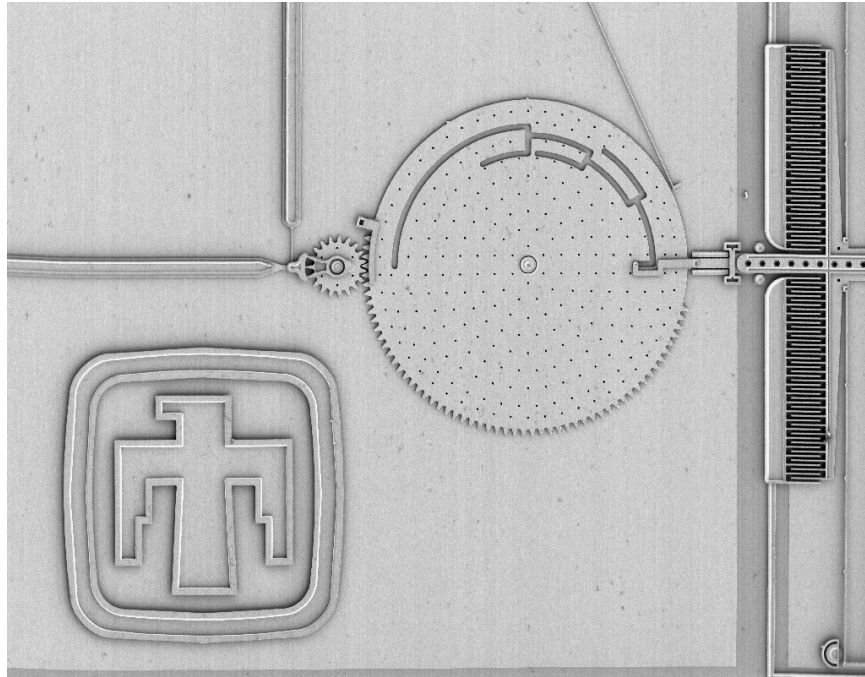


Figure 4. A pin-in-maze prototype mechanical discriminator built using polysilicon surface micromachining technology.

Use of photonic components to activate and power MEMS structures is of interest, because it allows for remote activation of the device, via optical fibers. Furthermore, this scheme provides for optical isolation, preventing inadvertent activation of a component and increasing surety of the system. The first demonstration consisted of powering a micro-mechanical pin-in-maze discrimination device with series-connected photovoltaic (PV) cells to produce 75 volts when illuminated with a fiber-coupled laser diode. Since each junction of a silicon photocell produces less than one volt, it was necessary to use PV arrays with a large number of coupled photocells to provide the 75 volts necessary to drive the MEMS component. The PV cells were mounted in the same package as the MEMS devices and wire-bonded to one of the electrostatic comb drives on the device. The MEMS device, a “pin-in-maze” discriminator, is shown in Figure 4. Note that the correct voltage (and thus amplitude of the laser light) must be supplied to the guide pin in order to successfully guide it through the maze and engage the gear drive mechanism. If an

incorrect value is supplied, the pin ends up in one of the “dead ends” of the maze and the gear drive is unable to rotate.

The control signals for the maze wheel were conventional electric signals, while the pin motion was controlled by the open circuit voltage of the PV cells; as modulated by a fiber-coupled laser diode. The 850 nm wavelength laser was able to “steer” the pin through the maze as the wheel rotated. The operation of this device demonstrates feasibility of optically isolating MEMS-based microsystem components and providing drive signals by transmission of optical power. Improvements are anticipated in both improving the efficiency and drive capabilities of series-connected photovoltaic cells and in reducing the drive voltage requirements of the MEMS actuators.

The second demonstration consisted of a micromachined device mechanically shuttering the beam from a VCSEL. Several fabrication and packaging challenges had to be overcome in order to implement the combined MEMS/photonic functionality.

The VCSEL was a design recently developed emitting at a wavelength of 1.06 microns³. At that long wavelength the silicon in the MEMS device is more transparent than at shorter wavelengths. The VCSEL was grown by metal-organic chemical vapor epitaxy (MOCVD) and consisted of three 80 Å thick InGaAs quantum wells with tensile strained GaAs_{0.8}P_{0.2} barriers embedded in 1-λ AlGaAs cavity. The bottom, n-type DBR consisted of 35 periods of GaAs/Al_{0.94}Ga_{0.06}As mirror pairs and the top, p-type contained 20 periods of GaAs/Al_{0.94}Ga_{0.06}As. The interfaces were graded parabolically in order to reduce the series resistance of the mirrors. To facilitate formation of the oxide aperture above and below the active region, layers of Al_{0.98}Ga_{0.02}As were grown immediately adjacent to the active region. The n-contact was made to the substrate with a AuGeNi alloy and the p-contact (TiPtAu) was made on top of the mesas with the center open for

the light to pass through. Figure 5 shows the electrical field distribution in the cavity of the VCSEL.

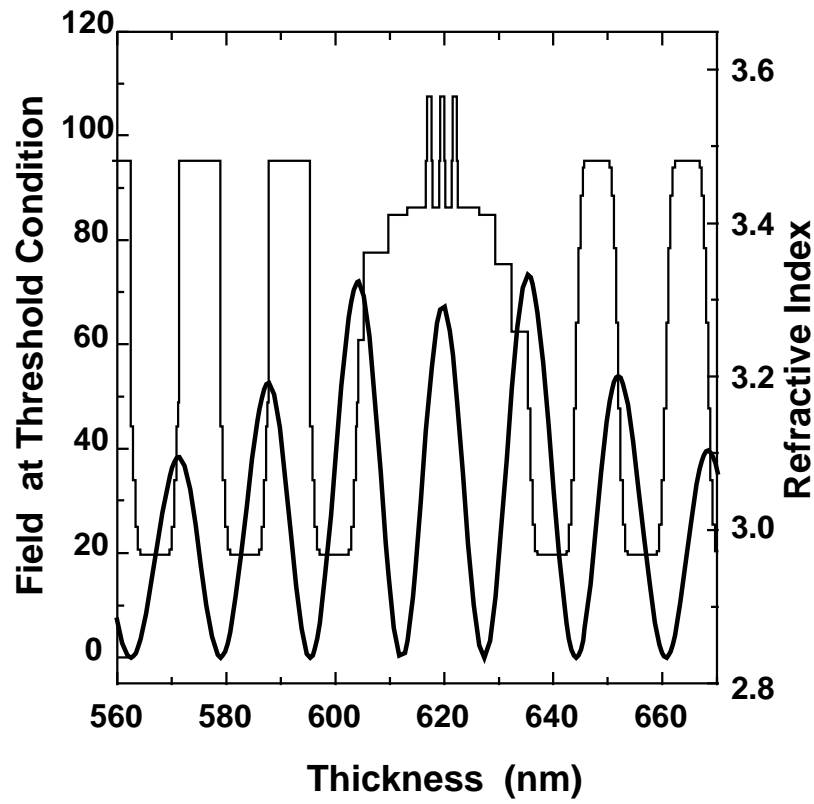


Figure 5. Structure of the active region of the 1.06 μm VCSEL and the electrical field distribution at threshold. The threshold is reached at a current of 7 mA and voltage of 1.5V, as illustrated in Figure 6.

The long wavelength of the VCSEL allows the laser beam to propagate through the silicon MEMS device substrate and, in the future, could enable the use of similar silicon MEMS structures to route optical signals to different parts of a chip.

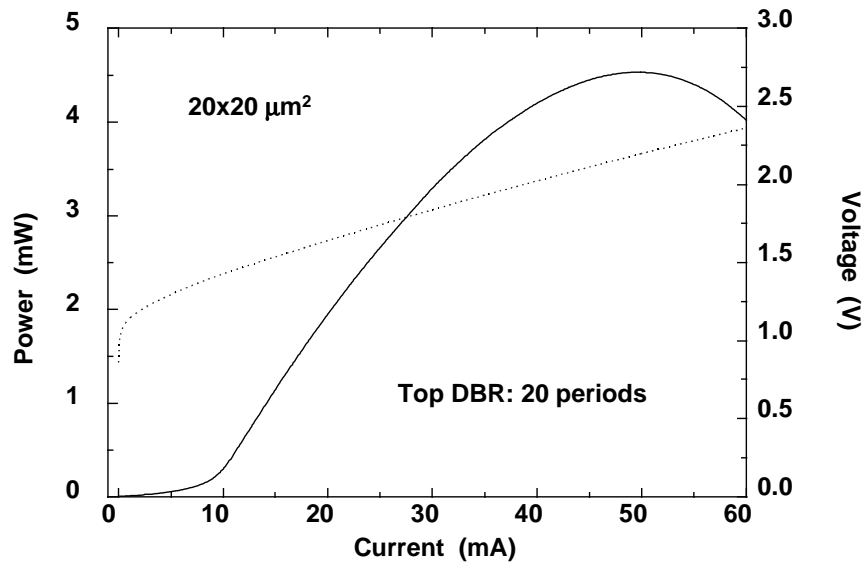


Figure 6. Light-current-voltage characteristic for the VCSEL. Light output is shown with a solid line using the left axis, whereas the voltage is shown with a dotted line using the right axis.

In order to ensure opaqueness to the VCSEL incident beam, gold was evaporated on the top surface of the mechanical shutter. One of the challenges in developing this capability was the development of a process to evaporate gold on a previously released MEMS structure without hindering its operation. Good adhesion and optical properties were achieved upon evaporation of 8 nm of Ti and 50 nm of Au. Another issue considered in the development of the process was stress-induced warpage of the wheel after evaporation. This issue was avoided through the use of a low temperature deposition process.

Finally, packaging issues for compatibility of both photonic and MEMS chips were addressed. A special hybrid package was assembled that allowed the VCSEL to be located close to the MEMS

device and enabled the entire optical beam to pass through the shutter aperture without auxiliary optics.

The resulting device is illustrated in Figure 7. Here the VCSEL light is visible through a hole in the gold-covered MEMS shutter. As drive voltages are applied to the electrostatic micromotor, the shutter rotates, thus periodically allowing the VCSEL to transmit through the device. Depending on the control signals, the shutter can rotate in either direction and at a variety of speeds. By thus blocking or passing a laser beam, the MEMS shutter can be used to enable transfer of signals or power by optical means.

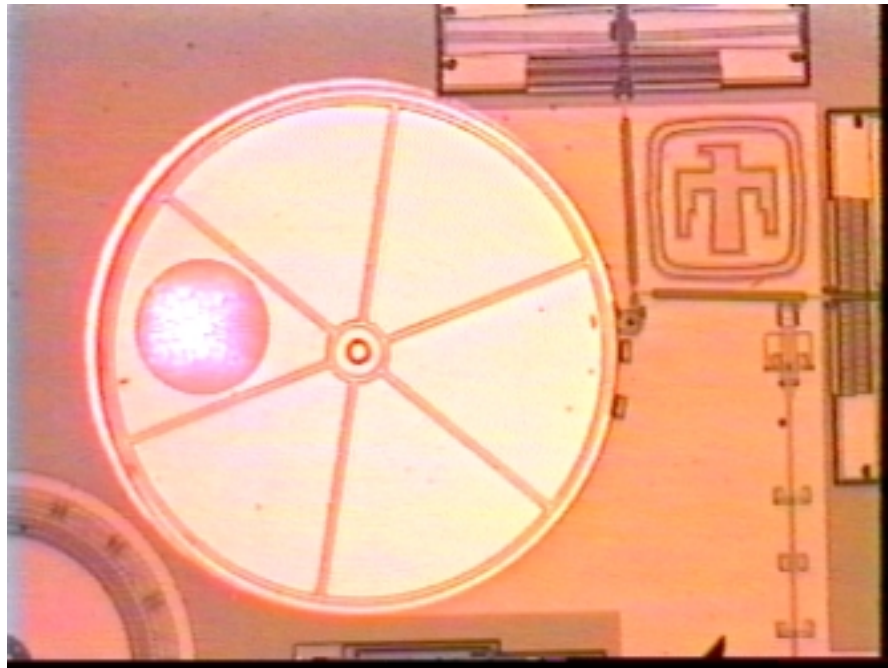


Figure 7. Top view of the metallized shutter and a VCSEL beam visible through a hole in that shutter.

Development of a Compact, MEMS-based Scanner

Low-speed laser scanning systems, in the range of 10Hz-1kHz can be used in a variety of applications including barcode scanners, video displays, laser print heads, and optical

communications. Enabling technologies for compact laser scanning systems are MEMS, optoelectronics and micro-optics. In this section, we report on the development of a compact laser scanning system which integrates these three technologies into a compact, manufacturable system. Part 2 of this section reviews the basic architecture of the integrated scanner system, while part 3 discusses design and fabrication issues for two generations of the silicon MEMS scanner. Part 4 discusses the design and fabrication of the micro-optical elements using direct-write electron beam lithography.

1. SYSTEM ARCHITECTURE

Micromachined scanning mirrors are an ideal choice for a compact laser scanner due to the small size, low power consumption and relative ease of integration with silicon microelectronics. Several groups have demonstrated manipulation of an on-chip laser beam using micromachined components^{4,5}. These devices often incorporate manually assembled MEMS prototypes coupled with laser diodes (typically edge-emitting) epoxied to the silicon MEMS substrate. While adequate for demonstration purposes, the assembly costs with this approach are prohibitively high. In the present work, a manufacturable alternative is pursued whereby the (VCSEL) light source and (MEMS) scanner are fabricated separately, and mounted onto a common fused silica substrate which serves as both an optical interconnect between the VCSEL and MEMS and as a component of the hybrid package. This approach, first demonstrated by Jahns and Huang⁶ is a way of integrating several optical components onto a single planar substrate for a small inexpensive optical system. To our knowledge, this is the first time this approach has been used to integrate free-space micromachined components with optoelectronic devices. Figure 8 illustrates the basic system architecture.

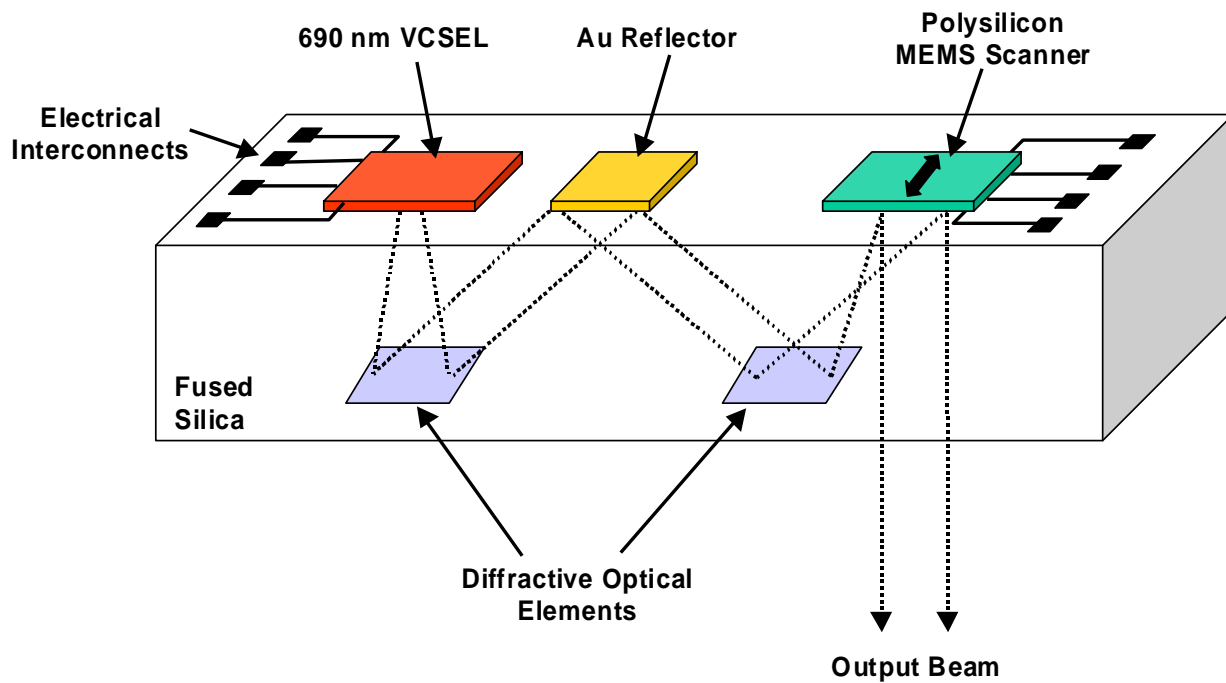


Figure 8. Basic system architecture of MEMS scanner with integrated VCSEL light source. Two DOEs are etched into the fused silica substrate, and a reflector patterned on the surface to direct the VCSEL beam toward the MEMS scanner.

Both the VCSEL and MEMS devices are bonded to the 2mm thick fused silica substrate using a precision alignment flip-chip bonder. Thermocompression bonds around the perimeter of the die form mechanical and electrical connection between the die and the fused silica substrate. This type of optical integration scheme has already been demonstrated by recent work on miniaturized chemical sensors⁷. By fabricating the MEMS and VCSEL devices separately, the two components can be optimized. Integration at a later time provides significant design and manufacturing flexibility. In addition, this architecture is scalable, allowing for additional components such as a photodetector or ASIC to be bonded to the fused silica substrate for greater functionality.

Two diffractive optical elements are etched into the fused silica surface to manage the VCSEL beam divergence and to increase the scan range. A diffractive optic is also etched into the polysilicon reflecting surface to collimate the output beam. Further detail on the design and fabrication of the optical components will be discussed below in part 4.

2. MEMS SCANNER DESIGN AND FABRICATION

Most scanning micromirrors fabricated with silicon surface micromachining are designed to be folded out of plane, and rotated about torsion springs or hinges^{8,9}, as shown schematically in Figure 9. The scan range is typically increased beyond the actuator displacement by relying on the lever arm formed by the close proximity of the torsion hinges to the actuator/mirror connection point. A requirement for the scanning mirror is that the surface of the polysilicon be extremely flat to prevent focussing of the beam which would degrade the resolution of the far field image. Recent work has shown that corrective optics can be used to partially compensate for curvature of the mirror caused by residual stress gradients in polysilicon⁹. However this would significantly increase the cost and complexity of an integrated laser scanning system. A second requirement is that the mirror must be very rigid to prevent dynamic deformation during operation. The torsion springs must also be made rigid enough to prevent significant translational motion during operation, which in turn requires either a high-force/high-frequency actuator or an actuator that operates at its resonant frequency.

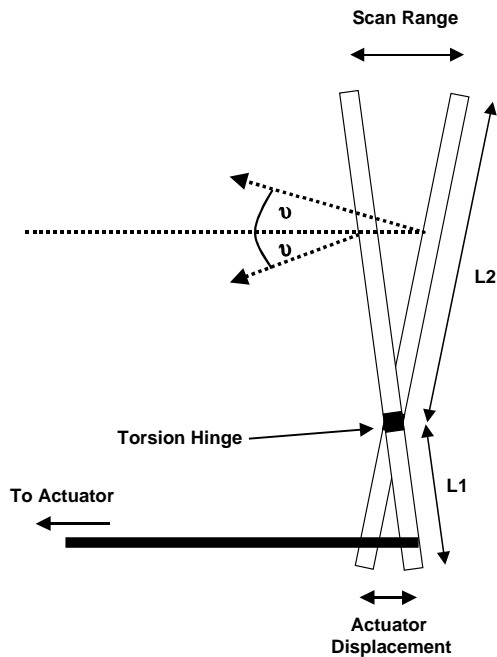


Figure 9. Schematic of typical raster scanning micromirrors using torsion hinges. The scanning range is increased by locating torsion hinges a distance $L1$ from mirror bottom, where $L1 < L2$.

3.1 First Generation MEMS Scanner

In the present work, an alternative device structure was investigated that would not lead to dynamic bending of the mirror surface and would not require corrective optics or an actuator operating at resonance. The first generation scanner design is shown below in Figure 10. The device was fabricated using Sandia National Laboratories Ultra-planar Multi-level MEMS Technology (SUMMiT), which is a four-level polysilicon MEMS technology. In the SUMMiT process, the sacrificial oxide below the fourth level of polysilicon is planarized using Chemical Mechanical Polishing (CMP), which removes the underlying topography from the top mirror surface producing a near-optically flat surface. Great care is taken during the SUMMiT fabrication process to reduce intrinsic stress in the mechanical polysilicon layers, and to reduce

local roughness. Typical values of local roughness due to polysilicon asperities are on the order of 1-5 nm rms.

The scanner shown in Figure 10 consists of a large 500 μm x 1000 μm polysilicon shuttle that moves in-plane by a linear rack attached to a rotary actuator. The rotary actuator is a microengine, developed at Sandia National Laboratories, consisting of two orthogonal electrostatic comb drives operating 90° out of phase to convert the linear movement of the comb drive to rotational motion. The bond pads and electrical leads to the comb drives were designed with overhanging ridges in the uppermost layer of polysilicon to prevent shorting of the electrical lines during the final blanket evaporation of gold (used to increase the reflectivity of the scanner surface). The microengine is capable of high-speed operation, in excess 100,000 rpm. However, the scanner developed in this work does not require high-speed operation. Thus an additional set of gears was added to serve as a microtransmission with a 12:1 gear reduction ratio. This will reduce the rotational speed by a factor of 12 with a corresponding increase in torque allowing for greater force to be transmitted to the linear rack and thus overcoming stiction of the large scanning shuttle. The advantage of using a linear rack is that the scan range can be increased by simply increasing the length of the rack and increasing the number of revolutions of the microengine, within the limits of springs attached to the shuttle. The 2 μm wide by 1100 μm long springs on the sides of the shuttle, as shown in

Figure 10, are fabricated using three mechanical layers of polysilicon, with a total thickness of 6.75 μm , providing out-of-plane rigidity but high in-plane compliance during operation. A conservative estimate for the resonant frequency of the microengine loaded by the mass-spring system of the shuttle is 314 Hz, which is above the intended operating frequency of 100 Hz. During operation, the scanner performed as intended providing smooth operation over the 100 μm scan range, at scan frequencies ranging from 1-100 Hz. However after several hundred cycles the devices tended to fail. The root cause has not yet been identified but wear debris generated by dimples contacting the top surface of the linear rack is proposed as a mechanism for producing discontinuous operation resulting in missed cycles.



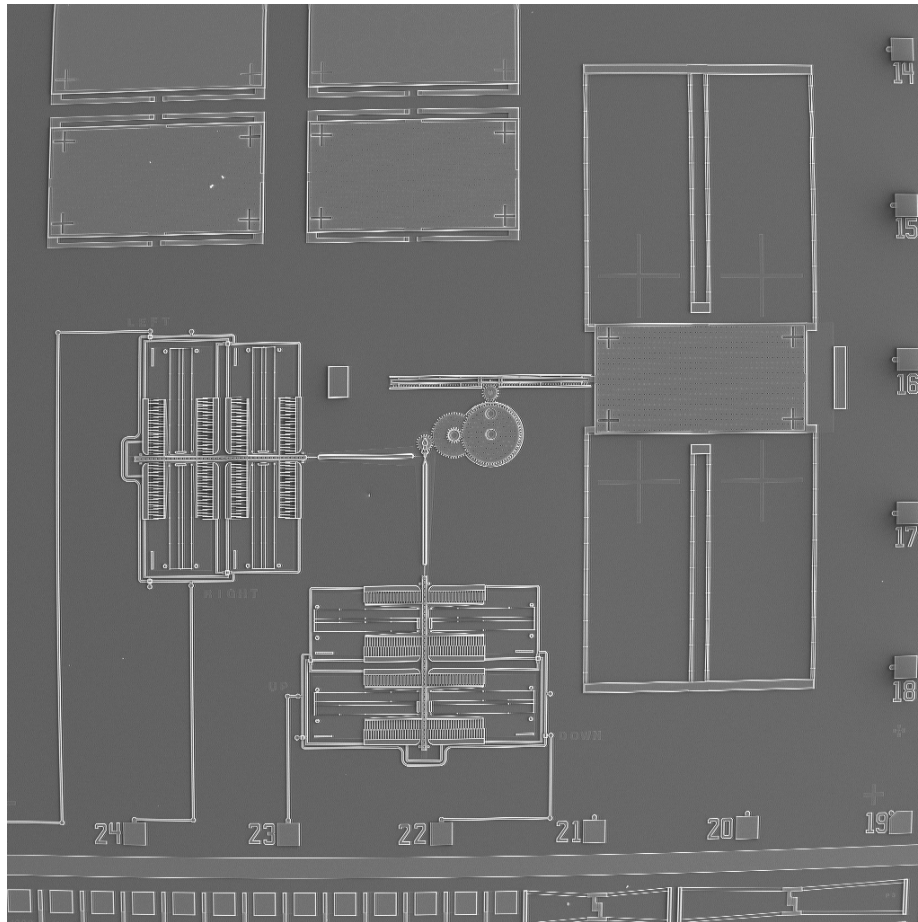


Figure 10. First generation scanner. A large polysilicon shuttle is displaced by a linear rack, which is driven by a microengine/microtransmission assembly.

Fig 11 is an SEM image of the $500\mu\text{m} \times 1000\mu\text{m}$ shuttle (without the diffractive optic) driven by the linear rack, showing the four springs attached to the corners of the shuttle. The large crosses in the corners serve as alignment marks for etching the diffractive optic into the surface of the polysilicon shuttle, and are outside the active area of the lens. Etch release holes were included in the mirror surface to remove the sacrificial oxide underneath. This is not expected to have a dramatic effect on the image quality, since diffraction orders will be outside the area scanned by the output beam. The etch release holes will decrease the efficiency of the device and is

estimated to result in a 2% loss. In the future, it may be possible to remove the sacrificial films from the backside of the mirror so as to eliminate the need for etch release holes. Once the diffractive optic is etched into the polysilicon shuttle, a 50 nm layer of gold (with a 8 nm Ti adhesion layer) is evaporated onto the surface to improve reflectivity.

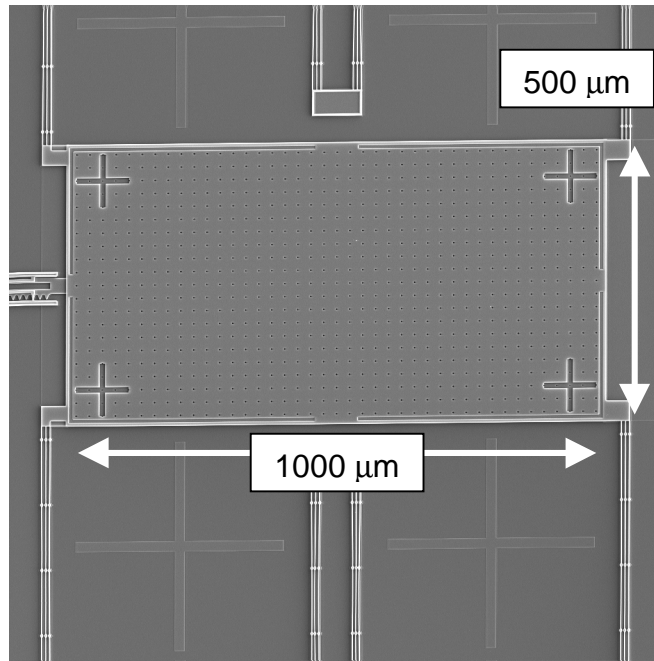


Figure 11. Gold-coated polysilicon shuttle used to manipulate the position of the output of a VCSEL light source.

An important consideration when using large polysilicon structures for optical surfaces is the curvature often found due to residual stress in the polysilicon films. In the case of reflective mirrors used for raster-scanning micromirrors, stress-induced curvature leads to defocussing of the beam, resulting in expansion of the far field image and a loss in resolution. For example, results were recently reported⁹ for an unmetallized 250 μm diameter micromirror fabricated at a commercial foundry in which the curvature of the polysilicon film resulted in a center to edge bow of about 1.2 μm. This degree of curvature resulted in a dramatic increase in the far field

beam area when compared to a perfectly flat mirror. This problem is usually compounded with the addition of metal on the mirror surface to improve reflectivity.

An effort was made in the present work to achieve as flat a surface as possible by fabricating the shuttle out of three mechanical layers of polysilicon. The total thickness of the polysilicon scanner shuttle is 4.75 μm . To quantify the flatness of this composite structure, z-axis displacement measurements were taken on a released device using a Wyco white light interferometer. The same polysilicon shuttle was measured before and after metallization. The metal coating again consisted of an 8 nm Ti adhesion layer, followed by a 50 nm layer of Au, both deposited by electron beam evaporation. The polysilicon mirrors without metal coatings were extremely flat, with less than 0.2 μm of center height. The mirrors with metal coatings showed much more curvature, with 0.56 μm center height with respect to the edge of the structure. This may be mitigated by further work on low stress metallic coatings.

3.2 Second Generation MEMS Scanner

As mentioned above, the first generation MEMS scanner had a tendency to fail after several hundred cycles, which is believed to be a result of wear in the linear rack component of the device. A second problem with this device is that the scan range was controlled by a set number of cycles output by the microengine before it reversed direction. If the linear rack briefly jammed while the microengine was running, the scanner would not be displaced the full amount before the microengine reversed direction. Thus, in the second generation scanner, a new design was investigated that would allow the actuator to run in a single direction while the shuttle scanned back and forth. Figure 12 shows an SEM image of the second generation scanner. The translation of the shuttle in Figure 12 is controlled by an arm connected to a large output gear from the microengine. As the gear rotates, the arm pushed the scanner shuttle back and forth. In this design the scan range is controlled by the diameter of the gear driving the scanning shuttle, which in this case was designed to give a 100 μm

displacement. One point to note in the design in Figure 12 is that a microtransmission was not used. By using an anti-stiction coating after releasing the structures, the high torque generated by the micro-transmission was not necessary to drive the $500\mu\text{m} \times 1000\mu\text{m}$ shuttle. Thus the design is capable of higher speed operation than the previous design, and provides much smoother operation. Work is currently underway to investigate the reliability of this design, but preliminary testing shows that this design is superior by demonstrating much more robust behavior. Future designs will incorporate larger output gears to increase scan range, and a 2D scanner based on the design in Figure 12 is also under development.

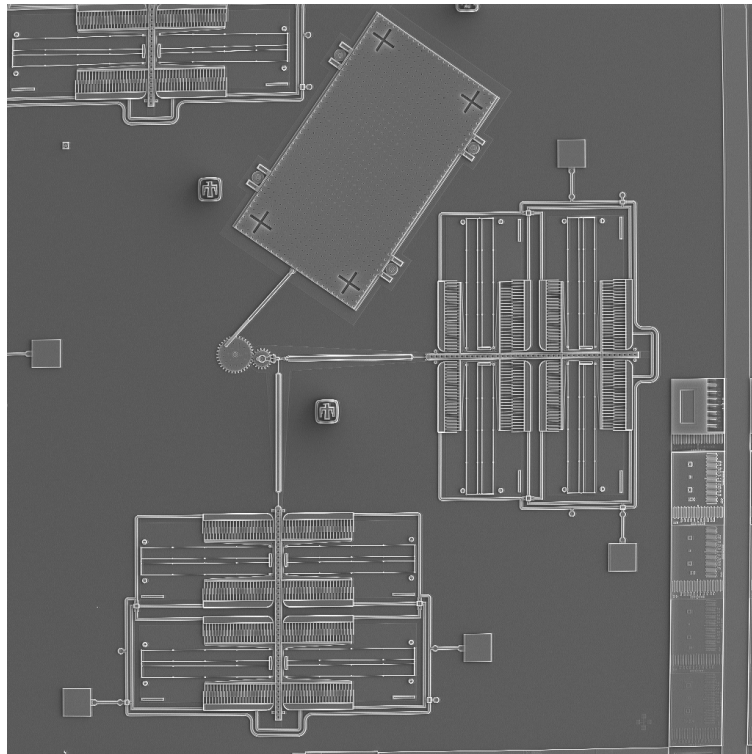


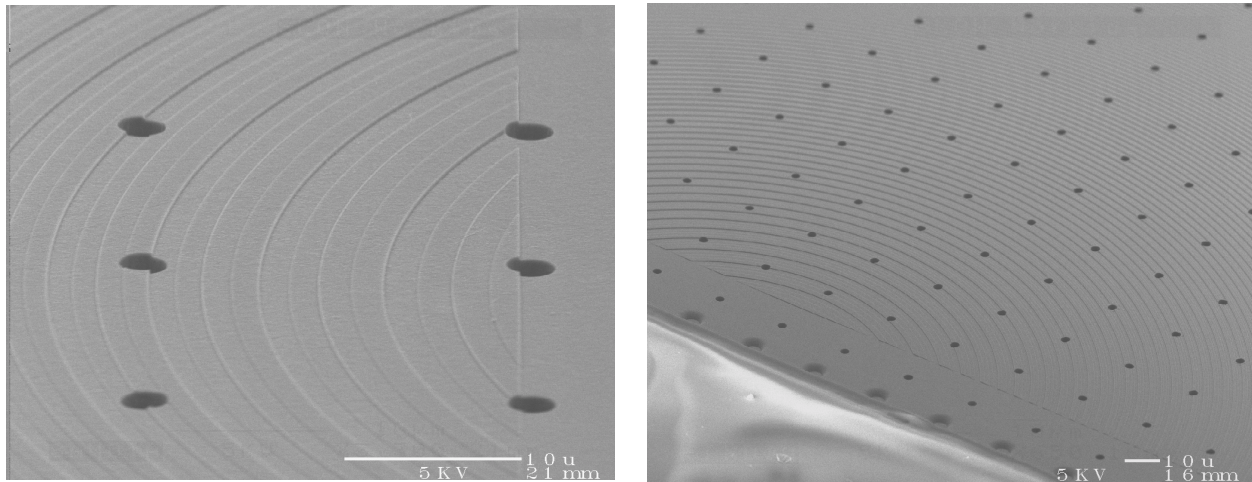
Figure 12. Second generation Optical MEMS scanner using single output gear on microengine.

3. OPTICAL SYSTEM DESIGN AND FABRICATION

The optical system is composed of two diffractive optical elements etched into a fused silica substrate and a third DOE etched into the shuttle of the MEMS scanner. The first two elements relay the beam to the scanner and size it appropriately. The first element collimates the 690-nm VCSEL output beam and tilts it about 20° so there will be room to mount both the VCSEL and the scanner. The second element retilts the beam slightly and focuses it in front of the third element. The third element, located on the scanner, produces a collimated output beam that is perpendicular to the substrate at the center of the scanner travel.

The system is designed such that the beam is about $500\ \mu\text{m}$ in diameter on all three diffractive elements. Thus the first two elements can be about $600\ \mu\text{m}$ in diameter and the third can be $600\ \mu\text{m}$ by $700\ \mu\text{m}$. We have chosen to make these binary DOEs with only four phase levels since for this technology demonstration, since fewer processing steps reduces the possibility of damaging the parts. With only four phase levels, the theoretical efficiency of each DOE is only 81%. But this is adequate for the intended purpose since $(81\%)^3 > 50\%$. Also, the minimum feature size for the elements is $0.25\ \mu\text{m}$ on the shuttle and slightly larger on the fused silica—this feature size can easily be written with optimized electron beam lithography. The fabrication challenges included dealing with the non-planar topography of the polysilicon MEMS structures and the need to process the devices prior to full release, but still have access to the surface of the shuttle surface. Special features were patterned into the shuttle surface to aid in the alignment of the electron-beam written pattern. The four-level diffractive lenses are etched directly into the fused silica substrate and the polysilicon scanner shuttle using Reactive Ion Beam Etching (RIBE), with nickel as the metal mask. The nickel mask is first defined using direct-write electron-beam lithography. Two scanning electron micrographs of portions of the shuttle with the DOE are shown in Figure 13. To our knowledge, this is the first demonstration of a multilevel DOE fabricated onto a surface-micromachined MEMS structure¹⁰.

The diffractive element on the scanner has a focal length of 700 μm and the total travel of the shuttle is 100 μm , therefore, the total scan angle is 0.14 radians which is ± 4 degrees or 8 degrees. The optical system is diffraction-limited on axis, and the resulting 0.5 mm spot size is roughly twice the diffraction limited size at the limits of its $\theta = \pm 4^\circ$ scan range. (Note that the shuttle must move perpendicular to the plane of the paper in Figure 8 or the aberrations will be much larger.)



Figures 13a and 13b. 13a (left) shows detail of the four etched levels of the DOE. The perforations facilitate the release etch that frees the shuttle for movement. 13b (right) shows the center edge of the polysilicon shuttle. The direction of motion of the shuttle is along the edge that is shown.

Conclusions

Significant progress was made in this project in combining MEMS technology with optoelectronic devices to realize optomechanical microsystems. The postprocessing techniques that have been developed have already proved useful for developing new microsystem concepts. Demonstrations of remote powering of MEMS devices with optical energy and simple optical MEMS components have been performed. Preliminary results on the design, fabrication and

testing of the components for a compact optical MEMS scanner are presented. The basic system architecture was reviewed for a laser scanning system integrating a VCSEL light source, diffractive optics and a polysilicon MEMS scanner into a compact hybrid package that is believed to be a more manufacturable alternative to previously reported designs. Two generations of MEMS scanners are presented, demonstrating smooth operation at the intended frequency of 100 Hz¹¹. Interferometric measurements show that the 500 μ m x 1000 μ m scanner shuttle is extremely flat in these designs, with a center to edge deflection of only 0.18 μ m over the ~400x900 μ m² active area for the unmetallized case, and 0.56 μ m for the metallized case. Innovative postprocessing of the MEMS scanner components have shown a first demonstration of high performance multilevel diffractive optical elements fabricated on moving polysilicon parts.

References

- ¹ R.J. Shul, C.G. Willison, and L. Zhang, Proceedings SPIE, **3511**, 252 (1998).
- ² O. Blum, M.E. Warren, H.Q. Hou, R.F. Carson, K.D. Choquette, M.S. Rodgers and J.J. Sniegowski, Proceedings SPIE, **3286**, 57, (1998).
- ³ H.Q. Hou, K.D. Choquette, K.M. Geib and B.E. Hammons, IEEE Photonics Lett. **9**, 1057 (1997).
- ⁴ M. Ikeda, et.al., Transducers 95, **1**, Stockholm Sweden, 293 (1995).
- ⁵ M.C. Wu, L.Y. Lin, S.S. Lee, K.S.J. Pister, Sensors and Actuators A, **50**, 127 (1995).
- ⁶ J.J. Jahns and A. Huang, Applied Optics, **28**, 1602 (1989).
- ⁷ M.E. Warren, et.al., Proceedings SPIE, **3878**, 185 (1999).
- ⁸ M.H. Kiang, O. Solgaard, R.S. Muller, IEEE J. MEMS, **7**, 27 (1998).
- ⁹ P.M. Hagelin, O. Solgaard, IEEE J. Selected Topics in Quantum Electronics, **5**, 67 (1999).
- ¹⁰ J.R. Wendt, G.A. Vawter, O. Blum, M.E. Warren, W.C. Sweatt, T.W. Krygowski and D. Reyes, J. Vacuum Sci. and Tech. B, to be published 2000.
- ¹¹ T.W. Krygowski, et.al., Proceedings SPIE, **3878**, 20 (1999).

DISTRIBUTION

3	MS 0603	Mial Warren (01743)
3	MS 0603	Olga Spahn(01743)
3	MS 0603	Bill Sweatt(01743)
3	MS 0603	Randy Shul(01743)
3	MS 0603	J.R. Wendt(01743)
3	MS 0603	G.A. Vawter(01742)
3	MS 1080	Tom Krygowski(01749)
3	MS 1080	David Reyes(01749)
3	MS 1080	Steve Rodgers(01749)
3	MS 1080	Jeff Sniegowski(01749)
1	MS 0612	Review and Approval Desk (09612) For DOE/OSTI
2	MS 0899	Technical Library (09616)
1	MS 9018	Central Technical Files (08940-2)